Optical nanofocusing by tapering coupled photonic-plasmonic waveguides

Xiaolong He,[1,2] Liu Yang,[1,2] and Tian Yang[1,*]

[1]University of Michigan- Shanghai Jiao Tong University Joint Institute, National Key Laboratory of Nano/Micro Fabrication Technology, Key Laboratory for Thin Film and Microfabrication of the Ministry of Education, State Key Lab of Advanced Optical Communication Systems and Networks, Shanghai Jiao Tong University, Shanghai 200240, China

[2]Equal contribution to this work

**tianyang@sjtu.edu.cn*

Abstract: We have numerically designed a compact structure to concentrate optical waves from a silicon-on-insulator waveguide to a deep sub-wavelength and high intensity surface plasmon focal spot at the tip of a metallic strip taper. A systematic design approach is developed to obtain an optimal photon-surface plasmon side coupling efficiency of up to 50% at 1.55 μm wavelength, and an over 50 times increase in electric field intensity in a focal region of around 20nm × 20nm × 7nm in size. The length of the whole device is 2.2 μm. We expect fabrication of the proposed device to be simpler than devices in previous work.

OCIS codes: (130.2790) Guided waves; (240.6680) Surface plasmons; (250.5403) Plasmonics.

References and links

1. E. Ozbay, "Plasmonics: merging photonics and electronics at nanoscale dimensions," Science **311**(5758), 189–193 (2006).
2. R. Zia, J. A. Schuller, A. Chandran, and M. L. Brongersma, "Plasmonics: the next chip-scale technology," Mater. Today **9**(7-8), 20–27 (2006).
3. L. Liu, Z. Han, and S. He, "Novel surface plasmon waveguide for high integration," Opt. Express **13**(17), 6645–6650 (2005).
4. S. I. Bozhevolnyi, V. S. Volkov, E. Devaux, and T. W. Ebbesen, "Channel plasmon-polariton guiding by subwavelength metal grooves," Phys. Rev. Lett. **95**(4), 046802 (2005).
5. R. F. Oulton, V. J. Sorger, D. A. Genov, D. F. P. Pile, and X. Zhang, "A hybrid plasmonic waveguide for subwavelength confinement and long-range propagation," Nat. Photonics **2**(8), 496–500 (2008).
6. D. Dai and S. He, "A silicon-based hybrid plasmonic waveguide with a metal cap for a nano-scale light confinement," Opt. Express **17**(19), 16646–16653 (2009).
7. T. Nikolajsen, K. Leosson, and S. I. Bozhevolnyi, "Surface plasmon polariton based modulators and switches operating at telecom wavelengths," Appl. Phys. Lett. **85**(24), 5833–5835 (2004).
8. K. F. MacDonald, Z. L. Sámson, M. I. Stockman, and N. I. Zheludev, "Ultrafast active plasmonics," Nat. Photonics **3**(1), 55–58 (2009).
9. J. N. Caspers, N. Rotenberg, and H. M. van Driel, "Ultrafast silicon-based active plasmonics at telecom wavelengths," Opt. Express **18**(19), 19761–19769 (2010).
10. T. Ishi, J. Fujikata, K. Makita, T. Baba, and K. Ohashi, "Si nano-photodiode with a surface plasmon antenna," Jpn. J. Appl. Phys. **44**(12), L364–L366 (2005).
11. L. Tang, S. E. Kocabas, S. Latif, A. K. Okyay, D.-S. Ly-Gagnon, K. C. Saraswat, and D. A. B. Miller, "Nanometre-scale germanium photodetector enhanced by a near-infrared dipole antenna," Nat. Photonics **2**(4), 226–229 (2008).
12. P. Neutens, P. Van Dorpe, I. De Vlaminck, L. Lagae, and G. Borghs, "Electrical detection of confined gap plasmons in metal-insulator-metal waveguides," Nat. Photonics **3**(5), 283–286 (2009).
13. A. Akbari, R. N. Tait, and P. Berini, "Surface plasmon waveguide Schottky detector," Opt. Express **18**(8), 8505–8514 (2010).
14. M. Hill, Y.-S. Oei, B. Smalbrugge, Y. Zhu, T. De Vries, P. J. Van Veldhoven, F. W. M. Van Otten, T. J. Eijkemans, J. P. Turkiewicz, H. De Waardt, E. J. Geluk, S.-H. Kwon, Y.-H. Lee, R. Nötzel, and M. K. Smit, "Lasing in metallic-coated nanocavities," Nat. Photonics **1**(10), 589–594 (2007).
15. C.-Y. Lu, S.-W. Chang, S. L. Chuang, T. D. Germann, and D. Bimberg, "Metal-cavity surface-emitting microlaser at room temperature," Appl. Phys. Lett. **96**(25), 251101 (2010).

#144631 - $15.00 USD Received 22 Mar 2011; revised 26 May 2011; accepted 10 Jun 2011; published 20 Jun 2011

16. R. F. Oulton, V. J. Sorger, T. Zentgraf, R.-M. Ma, C. Gladden, L. Dai, G. Bartal, and X. Zhang, "Plasmon lasers at deep subwavelength scale," Nature **461**(7264), 629–632 (2009).
17. M. A. Noginov, G. Zhu, A. M. Belgrave, R. Bakker, V. M. Shalaev, E. E. Narimanov, S. Stout, E. Herz, T. Suteewong, and U. Wiesner, "Demonstration of a spaser-based nanolaser," Nature **460**(7259), 1110–1112 (2009).
18. K. B. Crozier, A. Sundaramurthy, G. S. Kino, and C. F. Quate, "Optical antennas: resonators for local field enhancement," J. Appl. Phys. **94**(7), 4632–4642 (2003).
19. J. A. Schuller, E. S. Barnard, W. Cai, Y. C. Jun, J. S. White, and M. L. Brongersma, "Plasmonics for extreme light concentration and manipulation," Nat. Mater. **9**(3), 193–204 (2010).
20. E. Verhagen, A. Polman, and L. K. Kuipers, "Nanofocusing in laterally tapered plasmonic waveguides," Opt. Express **16**(1), 45–57 (2008).
21. E. Verhagen, M. Spasenović, A. Polman, and L. K. Kuipers, "Nanowire plasmon excitation by adiabatic mode transformation," Phys. Rev. Lett. **102**(20), 203904 (2009).
22. S. A. Maier, P. E. Barclay, T. J. Johnson, M. D. Friedman, and O. Painter, "Low-loss fiber accessible plasmon waveguide for planar energy guiding and sensing," Appl. Phys. Lett. **84**(20), 3990 (2004).
23. S. A. Maier, M. D. Friedman, P. E. Barclay, and O. Painter, "Experimental demonstration of fiber-accessible metal nanoparticle plasmon waveguides for planar energy guiding and sensing," Appl. Phys. Lett. **86**(7), 071103 (2005).
24. W. Ding, S. R. Andrews, and S. A. Maier, "Internal excitation and superfocusing of surface plasmon polaritons on a silver-coated optical fiber tip," Phys. Rev. A **75**(6), 063822 (2007).
25. D. E. Chang, A. S. Sørensen, P. R. Hemmer, and M. D. Lukin, "Quantum optics with surface plasmons," Phys. Rev. Lett. **97**(5), 053002 (2006).
26. D. E. Chang, A. S. Sørensen, P. R. Hemmer, and M. D. Lukin, "Strong coupling of single emitters to surface plasmons," Phys. Rev. B **76**(3), 035420 (2007).
27. L. Chen, J. Shakya, and M. Lipson, "Subwavelength confinement in an integrated metal slot waveguide on silicon," Opt. Lett. **31**(14), 2133–2135 (2006).
28. J. Tian, S. Yu, W. Yan, and M. Qiu, "Broadband high-efficiency surface-plasmon-polariton coupler with silicon-metal interface," Appl. Phys. Lett. **95**(1), 013504 (2009).
29. X. Guo, M. Qiu, J. Bao, B. J. Wiley, Q. Yang, X. Zhang, Y. Ma, H. Yu, and L. Tong, "Direct coupling of plasmonic and photonic nanowires for hybrid nanophotonic components and circuits," Nano Lett. **9**(12), 4515–4519 (2009).
30. F. Liu, R. Wan, Y. Li, Y. Huang, Y. Miura, D. Ohnishi, and J. Peng, "Extremely high efficient coupling between long range surface Plasmon polariton and dielectric waveguide mode," Appl. Phys. Lett. **95**(9), 091104 (2009).
31. R. Wan, F. Liu, X. Tang, Y. Huang, and J. Peng, "Vertical coupling between short range surface plasmon polariton mode and dielectric waveguide mode," Appl. Phys. Lett. **94**(14), 141104 (2009).
32. W.-P. Huang, "Coupled-mode theory for optical waveguides: an overview," J. Opt. Soc. Am. A **11**(3), 963–983 (1994).
33. E. D. Palik, *Handbook of Optical Constants of Solids*, Academic Press (1985).
34. Z. Y. Fang, L. R. Fan, C. F. Lin, D. Zhang, A. J. Meixner, and X. Zhu, "Plasmonic coupling of bow tie antennas with Ag nanowire," Nano Lett. **11**(4), 1676–1680 (2011).

1. Introduction

Since surface plasmon polaritons (SPPs) can be concentrated beyond the diffraction limit, SPP devices have been proposed as elements of future high density optoelectronic integrated circuits, in which the dimensions of the SPP elements can be small enough to match those of the integrated electronic elements [1,2]. Examples of such SPP elements include but are not limited to waveguides [3–6], switches and modulators [7–9], detectors [10–13], and lasers [14–17]. However, the ohmic losses of noble metals have hindered the development of all-plasmonic circuitry. It is more practical to guide the optical signals in low-loss dielectric waveguides and implement plasmonic components only for enhancing the interactions between optics and electronics such as optical-electrical and electrical-optical signal conversions. In this respect, optical antenna is a promising candidate. It has been widely explored for coupling free-space incident optical fields to highly concentrated and high intensity SPPs [11,18–21]. Co-directional coupling between optical fiber modes and SPPs has been demonstrated too [22–24]. But there have been fewer reports on concentrating guided optical waves to tiny bright SPP focal regions in planar circuits [25–28].

There are two approaches being actively sought for coupling planarly guided optical waves to SPPs: end-fire coupling [27–29], and side coupling [30,31]. In 2009, Tian *et al.* reported end-fire coupling between a tapered silicon waveguide and a metallic slot waveguide to nanofocus optical fields [28]. The devices were fabricated with a relatively complicated

#144631 - $15.00 USD Received 22 Mar 2011; revised 26 May 2011; accepted 10 Jun 2011; published 20 Jun 2011

procedure and the requirement on alignment precision was stringent. In the same year, Guo *et al.* reported in-plane side coupling between dielectric nanowires and metallic nanowires, with coupling lengths as short as several hundred nanometers [29]. The devices were fabricated with a nonscalable method. Also in 2009, Liu *et al.* reported an in-plane side coupling structure for converting optical waves in a silicon nitride waveguide to long range SPPs on a metallic waveguide, with a coupling efficiency of over 99% [30]. However, Liu's devices have dimensions of tens or hundreds of microns, which are too large for high integration density.

In this paper, we propose a compact and simple-to-fabricate device for planar lightwave nanofocusing, which is based upon vertical side coupling between optical waves and SPPs. It consists of a silicon-on-insulator (SOI) waveguide underneath a gold strip. Optical waves guided in the SOI waveguide are first coupled to SPPs on the gold strip. Then the whole structure is tapered to concentrate the SPPs to a deep sub-wavelength region, achieving an electrical field intensity more than 50 times higher than that in the SOI waveguide. A systematic design and optimization approach will be reported. This device proposal is important in that: i) it integrates coupling between optical waves and SPPs and nanofocusing of SPPs in one compact device; ii) fabrication of the proposed device is expected to be straightforward and simple, which is important for high-yield manufacturing of high integration density chips. Our design presents a practical and compact component for bridging the dimension gap between optics and electronics in planar circuits, and for significantly enhanced interactions between optics and nanoscale objects. Its potential applications include but are not limited to intra-chip optical interconnection and on-chip nano-optical biosensing.

2. Vertical side coupling between guided optical waves and SPPs

The configuration of the vertical side coupling structure that we propose is shown in Fig. 1(a). A dielectric waveguide, which is an SOI waveguide in this paper, and a SPP waveguide, which is a gold nano strip in this paper, are side-coupled to each other in the vertical direction. The coupling strength is controlled by the thickness of a silicon dioxide gap in between, which can be precisely controlled by material deposition techniques. The quasi-antisymmetric SPP waveguide mode of the gold nano strip is considered in this paper for coupling. It corresponds to the short range SPP mode if the gold strip is expanded into a metallic sheet with equal top and bottom cladding dielectric constants. In this paper, symmetry of modes is defined by the symmetry of the component of magnetic field which is parallel to the layer interfaces. By this definition, the quasi-antisymmetric SPP mode has anti-parallel magnetic field components at the top and bottom surfaces of the gold strip. This SPP mode is chosen because it becomes more focused but not cuts off when the gold strip is miniaturized, as shown in Ref [21]. This is crucial for nano focusing and is one of the fundamental differences from dielectric waveguide modes. On the other hand, the long range SPP mode on a metallic sheet corresponds to a quasi-symmetric mode on the gold nano strip, which is not considered in this paper because it does cut off when the gold strip is miniaturized. In the remainder of this section, we will follow a systematic approach to design the parameters of the structure in Fig. 1(a) to obtain an optimal coupling efficiency at 1.55 μm. We will first design an SOI waveguide and a gold strip which are phase matched to each other. Then we will optimize the coupling strength between them.

#144631 - $15.00 USD Received 22 Mar 2011; revised 26 May 2011; accepted 10 Jun 2011; published 20 Jun 2011

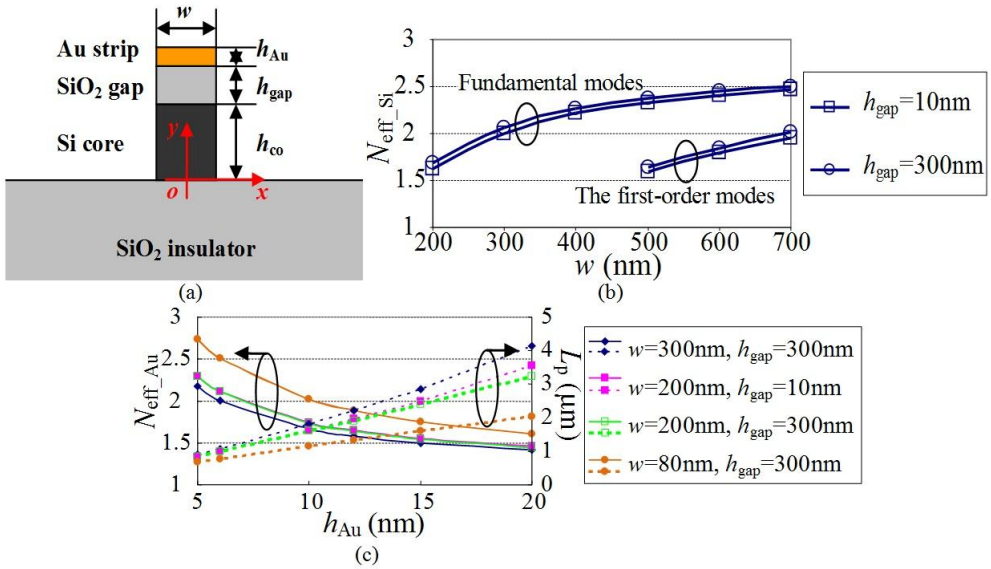

Fig. 1. (a) Cross-section of the vertical coupler. (b) The effective refractive index of the SOI waveguide mode, N_{eff_Si}, versus the silicon wire width, w, when the SOI waveguide is not coupled with the gold strip (by removing the gold strip from the structure). h_{co} = 300 nm. (c) The effective refractive index of the gold strip SPP mode, N_{eff_Au}, and its propagation length, L_p, versus the gold strip thickness, h_{Au}, where the gold strip is not coupled with the SOI waveguide (by replacing the silicon wire with silicon dioxide in the structure). h_{co} = 300 nm.

According to the coupled-mode theory, the phase mismatching factor (δ) should be zero to achieve efficient waveguide coupling [32]. That is, $\delta = (\beta_1 - \beta_2 + K_{11} - K_{22})/2 = 0$, where β_1 and β_2 are the real parts of the wave vectors of the two coupled waveguide modes, and K_{11} and K_{22} are the real parts of the self-coupling coefficients, respectively. In our design, the widths of the gold strip and the silicon wire are set to be the same unless otherwise specified, which not only simplifies device fabrication, but also make the mode sizes of the gold strip mode and the SOI waveguide mode close to each other. As a result, $K_{11} - K_{22}$ is small in our structure and will be ignored in the remainder of this paper, which will simplify our design process without significantly degradation in coupling performance. In the following, the structural parameters will be determined by the wave vector matching condition, which is $\beta_1 - \beta_2 = 0$, or equivalently the effective refractive index matching condition.

By the finite-difference method, we calculate the effective refractive indices of the SOI waveguide mode, N_{eff_Si}, and of the gold strip SPP mode, N_{eff_Au}, at 1.55 μm as shown in Fig. 1(b) and 1(c). Both modes are quasi-TM, whose major electric field components are in the *y* direction. The material refractive indices used in this work are taken from Ref [33], which are $n_{Au} = 0.559 - 9.81i$, $n_{Si} = 3.4764$, and $n_{SiO2} = 1.444$. The thickness of the silicon wire, h_{co}, is chosen as 300 nm, which is a typical thickness of single-mode SOI waveguides. The other structural parameters are chosen based upon the following observations. First, Figs. 1(b) and 1(c) show that the effective indices of the SOI waveguide and the gold strip SPP mode do not vary much with change of the silicon dioxide gap layer, so we will not consider the effect of gap thickness until when we calculate the coupling strength. Then Fig. 1(b) shows that in order for the fundamental mode of the SOI waveguide not to cut off, the silicon wire width, *w*, should not be smaller than around 200 nm. Figure 1(b) also shows that a larger *w* corresponds to a larger N_{eff_Si}, and from Fig. 1(c) this results in a thinner gold strip in order to satisfy the effective index matching condition, $N_{eff\_Au} = N_{eff\_Si}$. For example, w = 300 and 200 nm correspond to N_{eff_Si} = 2.03 and 1.65, which results in h_{Au} = 6 and 12 nm, respectively. However, Fig. 1(c) also shows that in a thinner gold strip, the ohmic loss is larger and the

#144631 - $15.00 USD Received 22 Mar 2011; revised 26 May 2011; accepted 10 Jun 2011; published 20 Jun 2011

propagation length, L_p, is shorter due to more power being confined inside metal. Therefore a narrower waveguide and a thicker gold strip are preferred for less SPP propagation loss. In the remainder of this paper, the structural parameters are taken to be h_{Au} = 12 nm, h_{co} = 300 nm and w = 200 nm, unless otherwise specified.

Next we shall choose the thickness of the silicon dioxide gap layer, which determines the coupling strength between the silicon wire and the gold strip. There are two eigenmodes of the coupled structure, which are approximately weighted sums of the uncoupled SOI waveguide mode and the gold strip SPP mode. One is a quasi even mode which we will call mode A, another is a quasi odd mode which we will call mode B. The major component of magnetic field, H_x, in the silicon wire is parallel to that in the gold strip in mode A, and anti-parallel in mode B, as shown in the left-side inset of Fig. 2(a). In order to find the thickness value of the silicon dioxide gap layer, h_{gap}, for efficient coupling between the silicon wire and the gold strip, we plot the effective indices and propagation distances of mode A and mode B as a function of h_{gap} in Fig. 2. The coupling length, $L_c = \lambda/2(N_{effA} - N_{effB})$ is also plotted. Figure 2(a) shows that when h_{gap} < 150 nm, mode B becomes leaky into the substrate. In addition, when h_{gap} is very small, coupling between the silicon wire and the gold strip is so strong that the coupled mode theory, which is based upon weak perturbation, is no longer valid. As an evidence, the right-side inset of Fig. 2(a) shows that when h_{gap} = 50nm, mode A becomes a hybrid plasmonic mode with electric field confined in the silicon dioxide gap [5,6]. On the other hand, as shown in Fig. 2(b), the coupling length increases with h_{gap}. Having a coupling length significantly shorter than the propagation distances of the eigenmodes is critical for achieving a high coupling efficiency. Therefore, we choose h_{gap} = 150 nm, with a corresponding coupling length, L_c, of 1.7 μm.

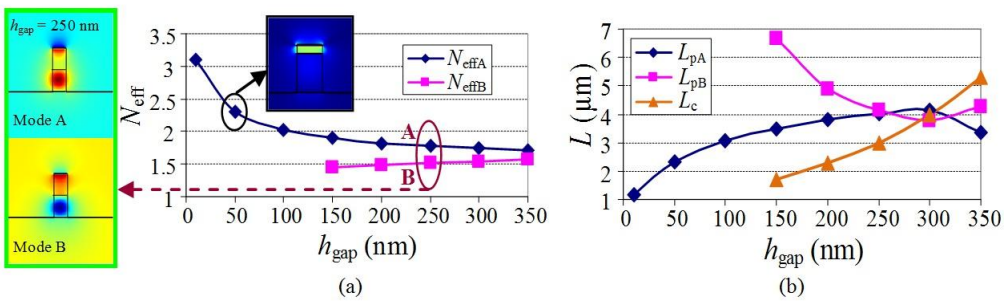

Fig. 2. (a) Effective indices of quasi-even mode A and quasi-odd mode B in a silicon wire - gold strip coupled structure with different gap thickness values h_{gap}. h_{Au} = 12 nm, h_{co} = 300 nm and w = 200 nm. The left inset shows the field profile real(H_x) of mode A and mode B when h_{gap} = 250 nm. The right inset shows the field profile $|E_y|$ of mode A when h_{gap} = 50 nm. (b) Propagation distances of mode A and mode B and corresponding coupling lengths.

With the optimal structural parameters chosen, we simulate the propagation of optical waves and SPPs in the coupled structure by the finite-difference time-domain (FDTD) method as shown in Fig. 3. The propagation begins with the fundamental mode of the SOI waveguide, and coupling to the gold strip starts at z = 0. Figure 3(a) shows the z-component of Poynting vector, P_z, in the plane x = 0. In Fig. 3(b), the normalized powers in the SOI waveguide mode and the gold strip SPP mode, P_{Si} and P_{Au}, are calculated by overlap integrals between the total field and the fields of uncoupled guided modes. The figures show that the power in the silicon wire gradually couples into the gold strip until z ≈1.8 μm, which is close to the designed coupling length L_c = 1.7 μm. The little difference comes from the phase difference between mode A and mode B at the beginning of coupling, where the total field is the SOI waveguide mode but not exactly (A-B). The extinction ratio, $10\log_{10}(P_{Au}/P_{Si})$, is around 20 dB at z ≈1.8 μm. This high extinction ratio confirms our earlier prediction that mismatch between the self coupling coefficients K_{11} and K_{22} is small enough so as not to

#144631 - $15.00 USD Received 22 Mar 2011; revised 26 May 2011; accepted 10 Jun 2011; published 20 Jun 2011

degrade the coupling performance. The power in the SPP mode reaches a maximum of 50% of launched power at z = 1.2 μm. This is a shorter distance than the coupling length due to metallic ohmic loss.

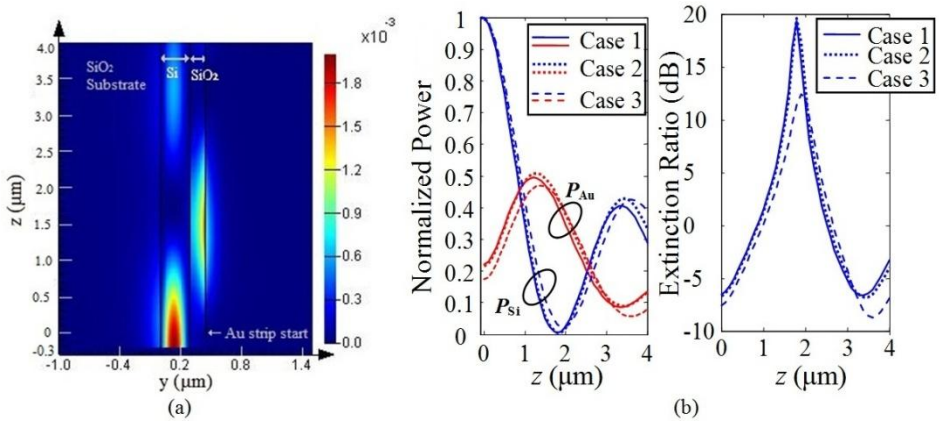

Fig. 3. Electromagnetic field propagation in a silicon wire - gold strip coupled structure, with the field beginning as the fundamental mode of the SOI waveguide. (a) The z-component of Poynting vector, P_z, in the plane x = 0. h_{Au} = 12 nm, h_{gap} = 150 nm, h_{co} = 300 nm and w = 200 nm. (b) Normalized powers in the SOI waveguide mode and the gold strip SPP mode along propagation, and the extinction ratio. Case 1 is the same structure as in Fig. 3(a). In Case 2 the width of the gold strip w_{Au} = 160 nm, and h_{Au} = 15 nm; in Case 3, w_{Au} = 100 nm, and h_{Au} = 20 nm; other structural parameters are not changed.

To investigate the effect of self-coupling coefficient mismatch, we do calculations for devices in which the width of the gold strip is different from that of the silicon wire, as shown by Case 2 and Case 3 in Fig. 3(b). The thicknesses of the gold strips are adjusted correspondingly to satisfy the β_1 - β_2 = 0 wave vector matching condition. Both the extinction ratio and the maximum coupling efficiency degrade when the gold strip is only half as wide as the silicon wire.

3. Nanofocusing

After the optical waves are converted to SPPs through coupling between the silicon wire and the gold strip, we taper down the whole structure to focus the SPPs into a nanoscale focal region. Figure 4(a) is a schematic diagram of the whole device containing both the coupling part and the tapered part. While, as in Fig. 3, in a non-tapered structure power couples back from the gold strip to the silicon wire after propagating for one coupling length L_c, back coupling is naturally removed in the tapered structure since the phase-matching condition is not satisfied in the tapered part. This can be predicted from Fig. 1: Fig. 1(b) shows that, when w is tapered to below 200 nm, the SOI waveguide supports no guided modes; Fig. 1(c) shows that the effective index of the antisymmetric SPP mode increases when w decreases. Therefore, if we taper down the width of the whole structure after the optical waves are coupled to SPPs, the SPPs will be confined around the gold strip without coupling back into the silicon wire [25,26]. It is interesting to notice that although a very strong coupling between the gold strip and the silicon wire might result in a higher coupling efficiency thanks to a very short coupling length, such as in Ref [29], it is unwanted in the tapered part since it would let the SPPs couple back into the SOI waveguide before being focused.

#144631 - $15.00 USD Received 22 Mar 2011; revised 26 May 2011; accepted 10 Jun 2011; published 20 Jun 2011

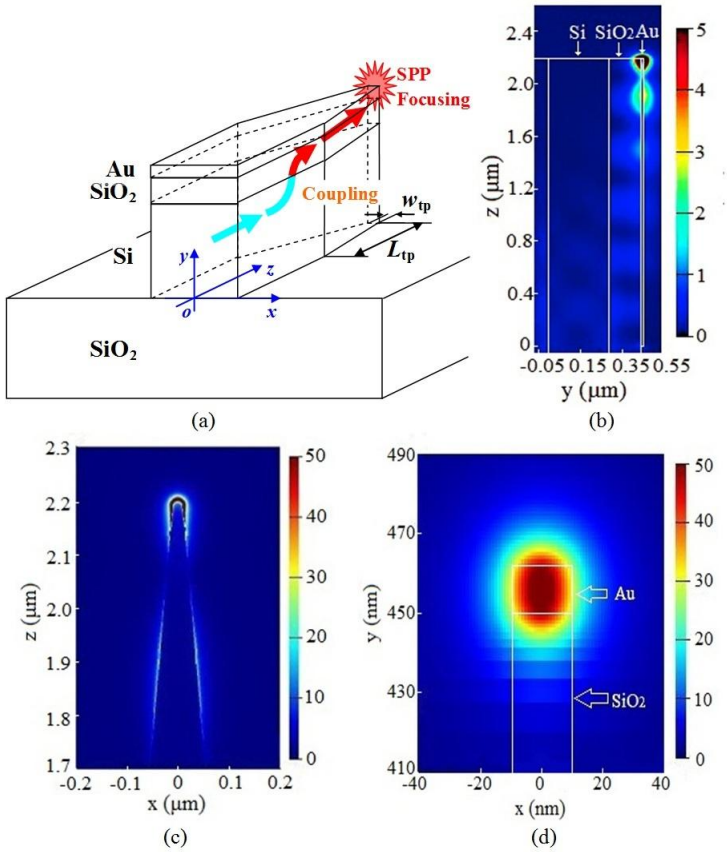

Fig. 4. Electric field intensity profile, $|E|^2$, of coupling between an SOI waveguide and a gold strip, and nanofocusing by tapering. The diameter of taper tip is 20nm. All $|E|^2$ values are normalized to the peak $|E|^2$ value of the SOI waveguide mode in the silicon wire. Color scales are saturated to improve visibility. (a) A schematic diagram of the device. (b) $|E|^2$ in the plane x = 0. (c) $|E|^2$ near the taper tip, at the bottom surface of the gold strip. (d) $|E|^2$ at 6nm in front of the taper tip.

We have simulated the coupling and nanofocusing processes by the FDTD method. The length of the coupling part is taken as 1.2 μm for maximum coupling from optical waves to SPPs before tapering starts. Then the structure width, w, is tapered down from 200 nm to w_{tp} = 20 nm within a taper length L_{tp} = 1 μm. The grid sizes of the simulation mesh are 5 nm × 1 nm × 10 nm in and close to the gold strip in the coupling part. The grid sizes gradually decrease to 1 nm × 1 nm × 0.5 nm around the tip of the taper. Figure 4(b) and 4(c) shows the electric field intensity, $|E|^2$, in the central cross section of the device, the plane of x = 0, and at the bottom surface of the gold strip taper, the plane of $y = h_{co} + h_{gap}$, respectively. It can be seen that with the optical waves launched in the SOI waveguide, the electric field is finally strongly focused at the tip of the gold nanotaper. Reflection from the end of the taper leads to an interference pattern along the device. As predicted, no significant back coupling is observed in the tapered part. Figure 4(d) shows the electric field intensity profile of the focal spot in an x-y plane in front of the taper tip, which is a nice single spot mainly polarized in the z direction. In a volume of around 20nm × 20nm × 7nm in front of the tip of the taper, the electric field intensity is over 50 times higher than the peak intensity of optical waves launched in the silicon wire. The electric field enhancement with a 1 μm long taper is higher than that with 0.8 μm and 1.2 μm long tapers in our calculation.

#144631 - $15.00 USD Received 22 Mar 2011; revised 26 May 2011; accepted 10 Jun 2011; published 20 Jun 2011

To investigate SPP propagation along the tapered gold strip and reflection off the taper tip, we plot optical powers at different *z* coordinates along the taper as in Fig. 5(a). Optical powers decrease along the *z* direction due to ohmic loss, radiation loss and reflection off the tip. As a comparison, we calculate the optical powers in a similar device, but in which the 20nm diameter taper tip is replaced by an infinitely long and 20nm wide strip, as shown in the inset of Fig. 5(b). The replacement of the half-circle shaped taper tip by an extended strip significantly reduces reflection. According to Fig. 5(b), at least 23% of the power launched in the silicon wire is delivered to the tip of the taper. Compared with Fig. 5(a), 92% of the power that reaches the tip is reflected backwards. If the tip reflection could be eliminated by placing an impedance matched load, the electric field intensity in the focal spot could be enhanced by a much greater factor than in Fig. 4 [34]. This is an interesting issue to be addressed in future work.

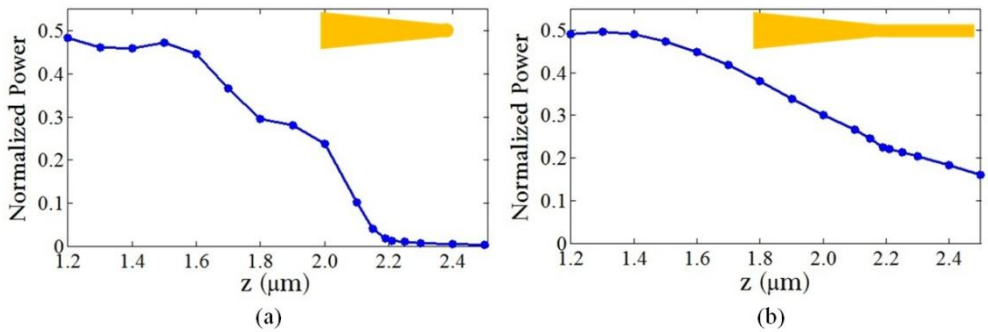

Fig. 5. Optical powers along *z* direction at different *z* coordinates. The power values are the powers flowing through rectangles which enclose the gold strip. The top (bottom) segments of the rectangles are 250nm (150nm) above (below) the top (bottom) surface of the gold strip, and the left (right) segments of the rectangles are 200nm to the left (right) border of the strip. (a) Optical powers along the tapered part of the device in Fig. 4. (b) Optical powers along a tapered device which has a 20nm wide gold strip extending from the end of the taper.

4. Conclusion

We have proposed a simple and compact device based upon vertical side coupling between an SOI nanowire waveguide and a gold nanostrip. The proposed device combines coupling between guided optical waves and SPPs and nanofocusing of SPPs. It is a promising candidate for scalable manufacturing on planar lightwave circuit chips to achieve efficient interactions between optics and nanoscale objects.

We have presented a systematic approach to design and optimize the performance of the proposed device at 1.55 μm. In an optimized device, 50% of the optical power launched in the silicon wire is coupled to SPPs on the gold strip within a coupling distance of 1.2 μm. By tapering the width of the whole device to 20 nm within a 1 μm taper length, the SPPs are focused to a deep sub-wavelength focal region, with over 50 times enhancement in electric field intensity in a volume of around 20nm × 20nm × 7nm. We anticipate a much greater enhancement of the focused electric field by eliminating reflection off the taper tip.

Acknowledgments

This work is supported by the Shanghai Pujiang Program under grant# 10PJ1405300, the Program for New Century Excellent Talents in University by the Ministry of Education of China, The National High Technology Research and Development Program of China (863 Program) under grant # 2011AA050518863, and the China Postdoctoral Science Foundation under grant# 20100470704.

#144631 - $15.00 USD Received 22 Mar 2011; revised 26 May 2011; accepted 10 Jun 2011; published 20 Jun 2011